S1: Control points of the Toce River case study

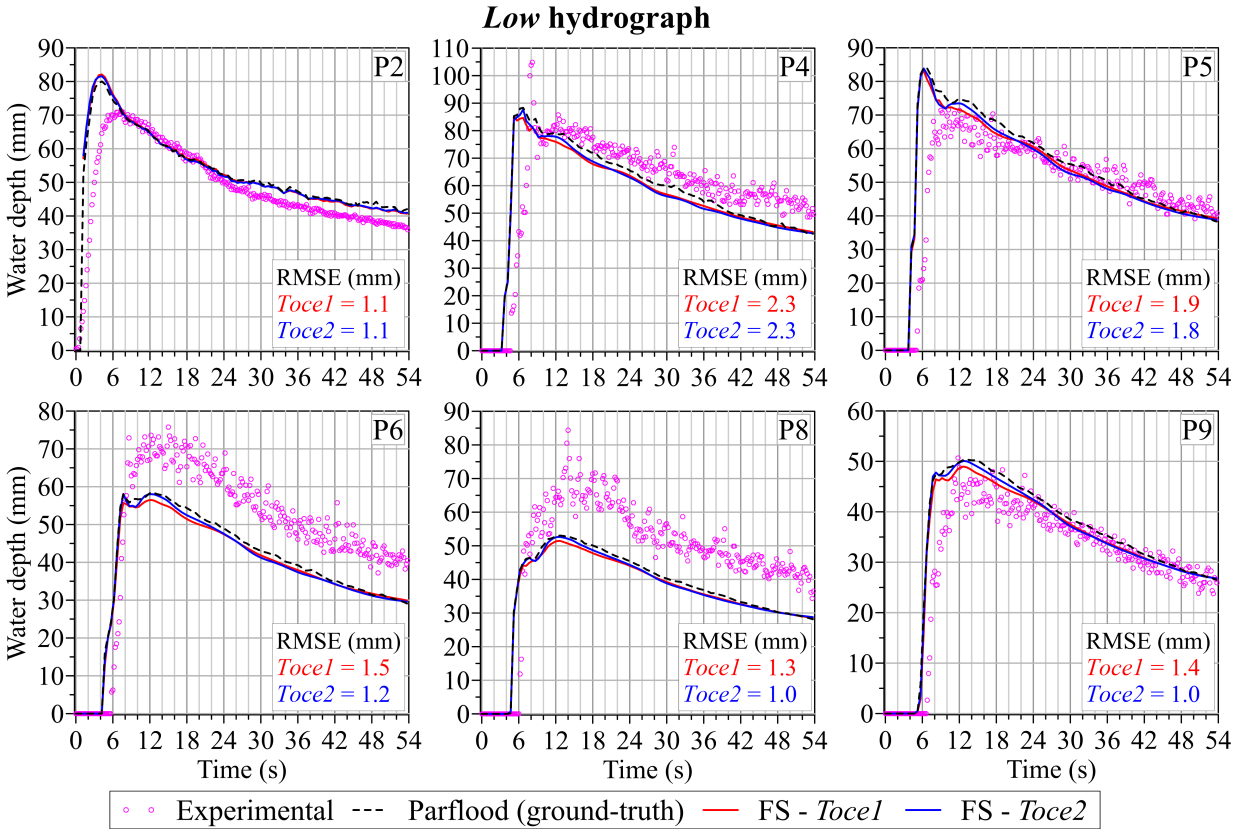

Figure S1. Toce River case study: water depths recorded and simulated at 6 control points (P2−P4−P5−P6−P8−P9) for the *Low* hydrograph of the testing dataset. The magenta circles represent the recorded water depths during the experimental analysis in the physical model (Testa et al., 2007). Each graph includes the RMSEs computed by comparing the time series of ground-truth and predicted water depths for both the *Toce1* and *Toce2* training configurations.

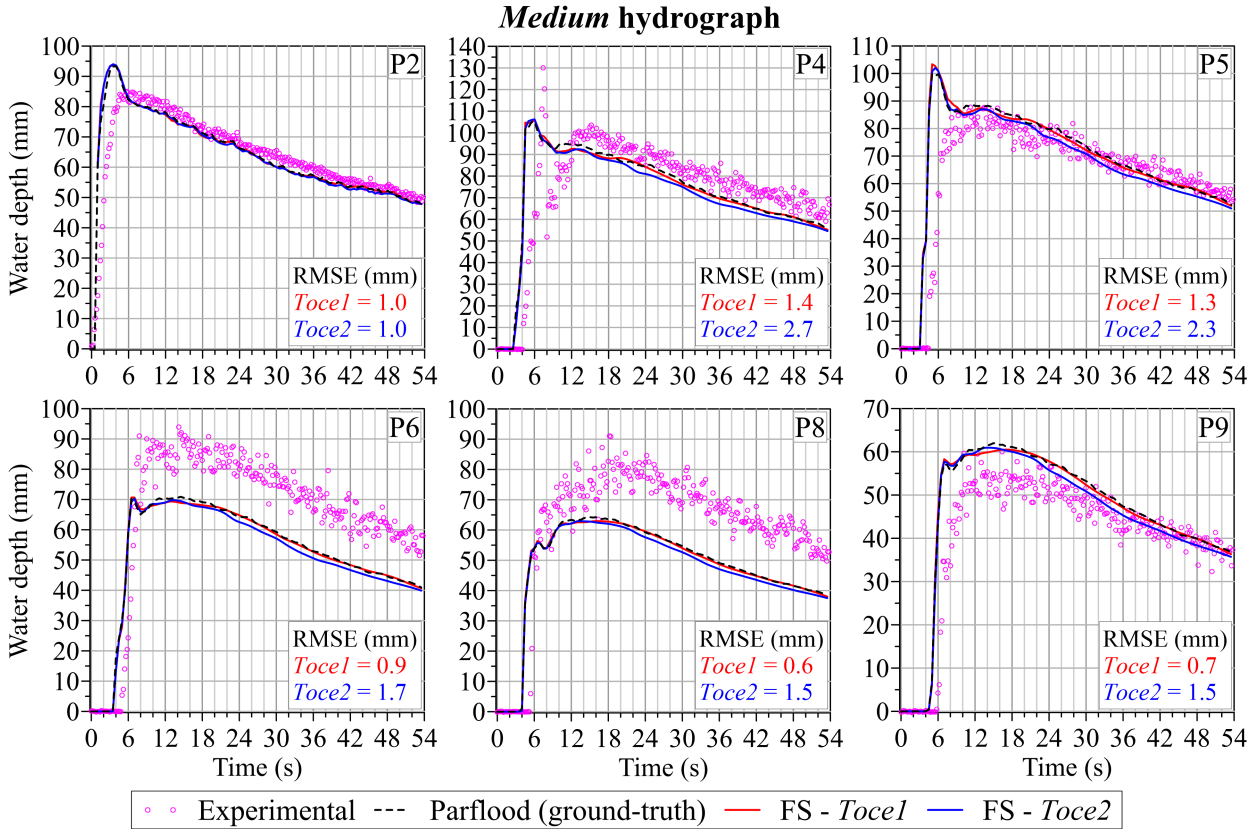

Figure S2. Toce River case study: water depths recorded and simulated at 6 control points (P2−P4−P5−P6−P8−P9) for the *Medium* hydrograph of the testing dataset. The magenta circles represent the recorded water depths during the experimental analysis in the physical model (Testa et al., 2007). Each graph includes the RMSEs computed by comparing the time series of ground-truth and predicted water depths for both the *Toce1* and *Toce2* training configurations.

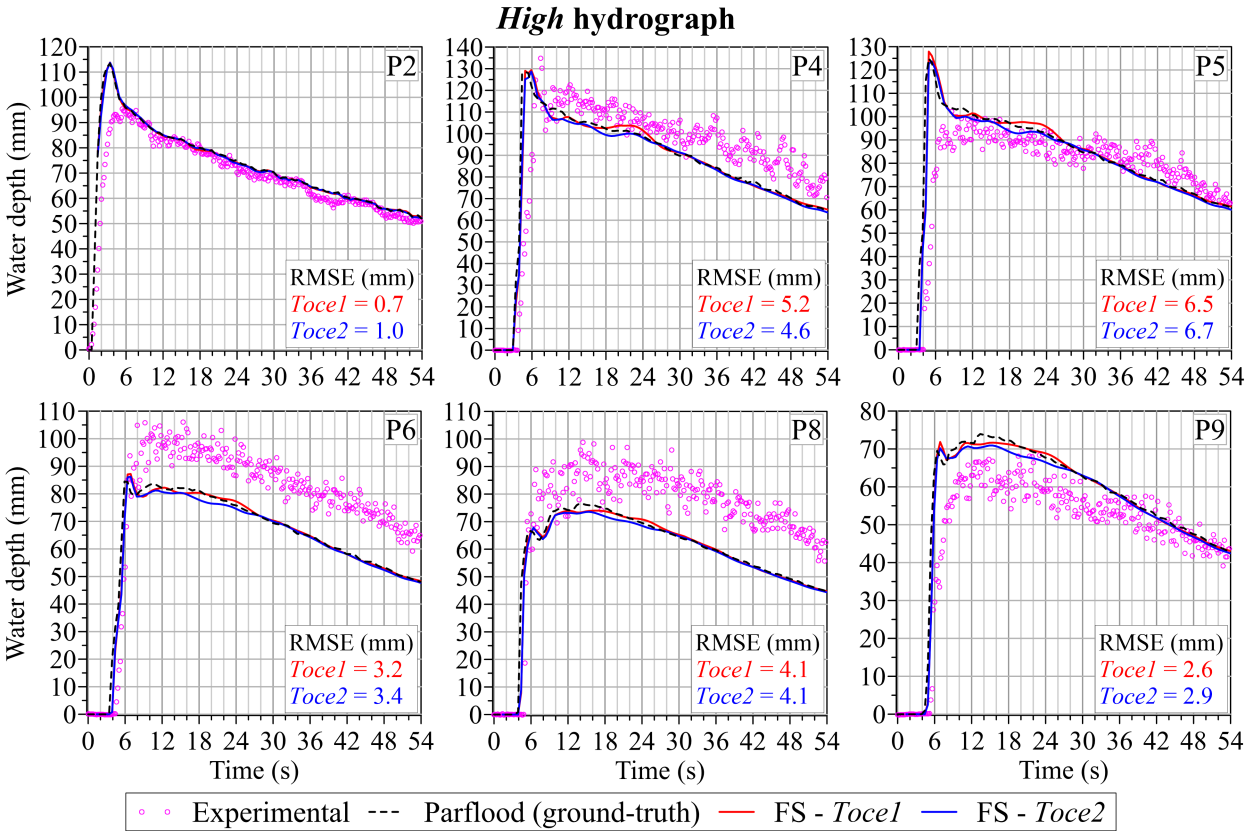

Figure S3. Toce River case study: water depths recorded and simulated at 6 control points (P2−P4−P5−P6−P8−P9) for the *High* hydrograph of the testing dataset. The magenta circles represent the recorded water depths during the experimental analysis in the physical model (Testa et al., 2007). Each graph includes the RMSEs computed by comparing the time series of ground-truth and predicted water depths for both the *Toce1* and *Toce2* training configurations.

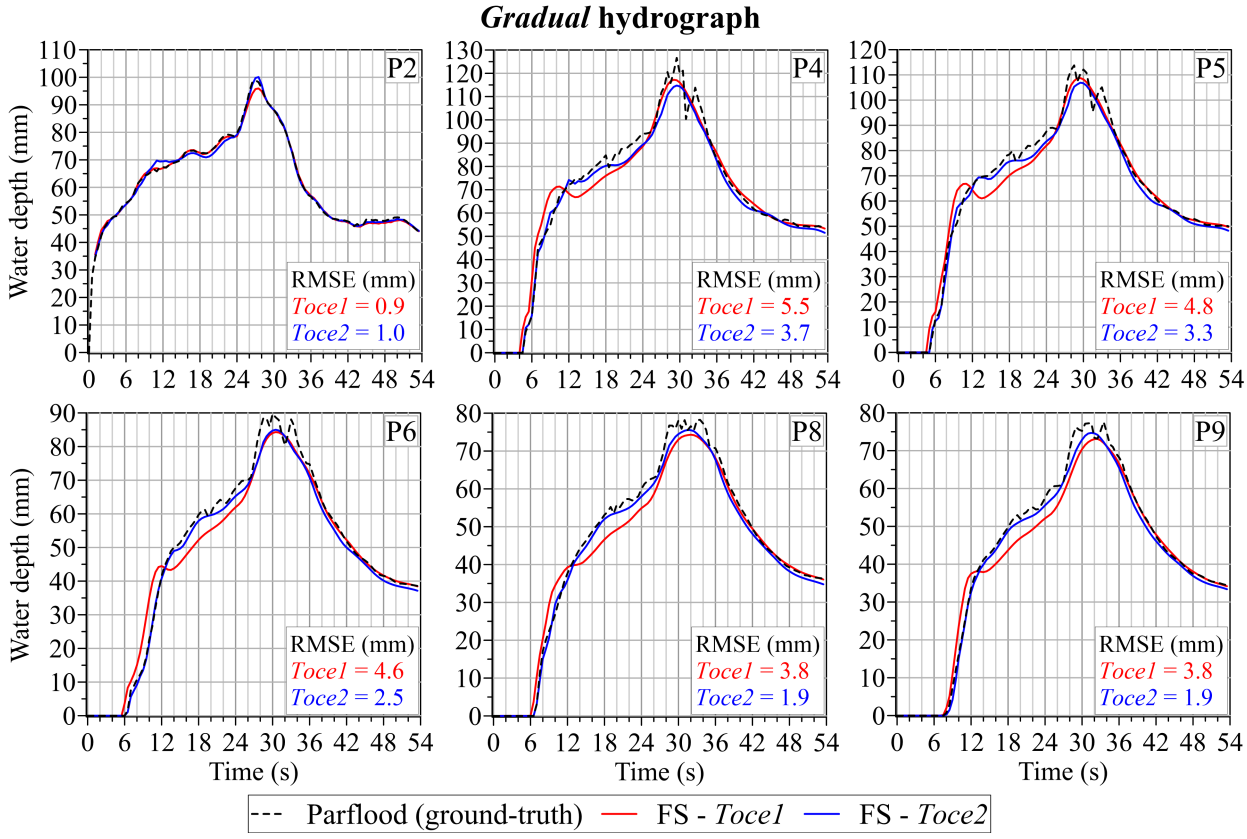

Figure S4. Toce River case study: water depths recorded and simulated at 6 control points (P2−P4−P5−P6−P8−P9) for the *Gradual* hydrograph of the testing dataset. Each graph includes the RMSEs computed by comparing the time series of ground-truth and predicted water depths for both the *Toce1* and *Toce2* training configurations.

S2: Toce River case study: inundation maps for different training configurations

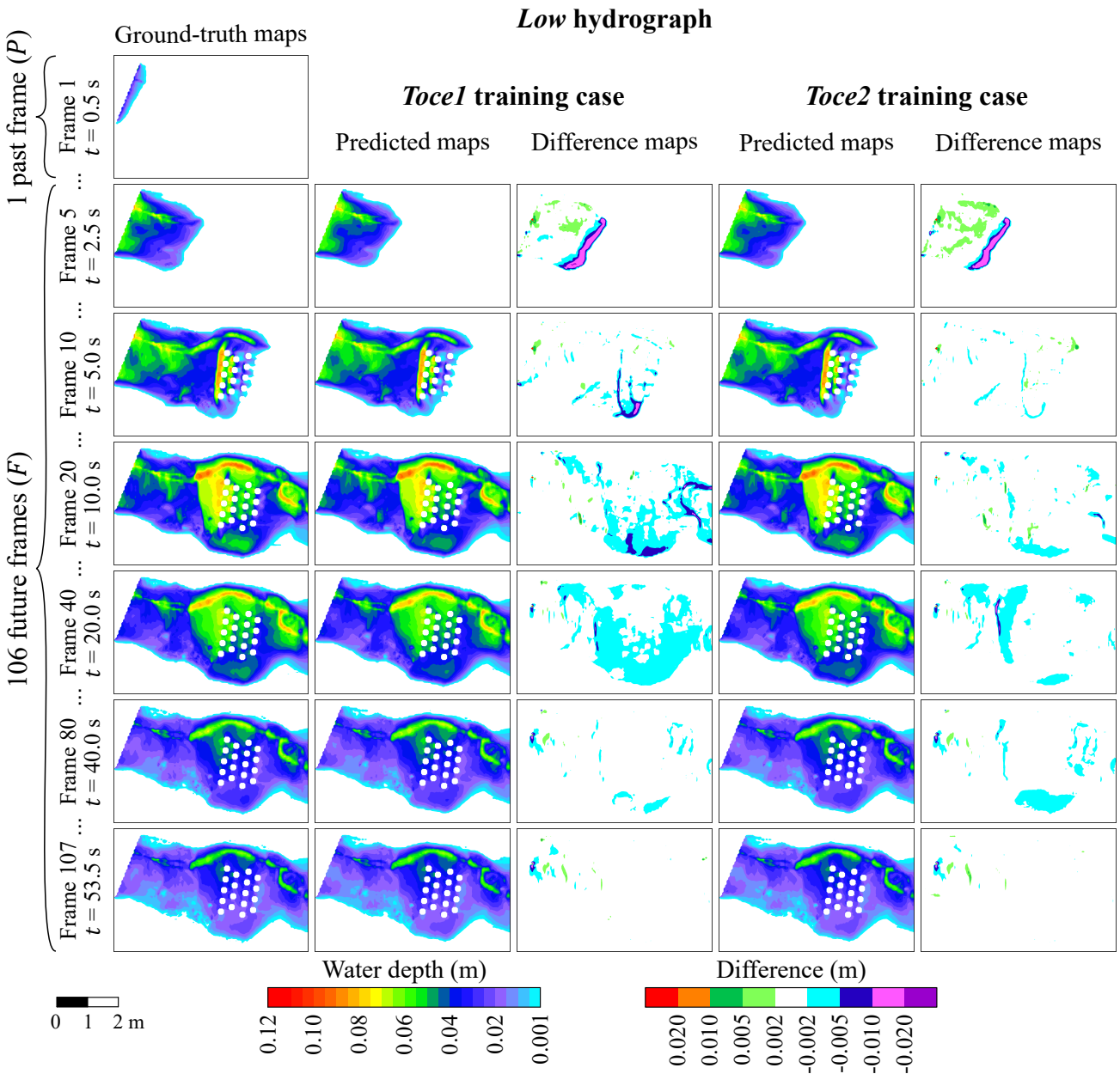

Figure S5. Toce River case study: comparison of predicted maps for the *Low* hydrograph of the testing dataset using the surrogate model trained with the *Toce1* and *Toce2* configurations. The first column presents the ground-truth maps obtained from the hydrodynamic model. The second and fourth columns show the predicted maps for the *Toce1* and *Toce2* configurations, respectively. The third and fifth columns illustrate the differences between the predicted and target maps for the *Toce1* and *Toce2* configurations, respectively. Only selected representative instants are shown.

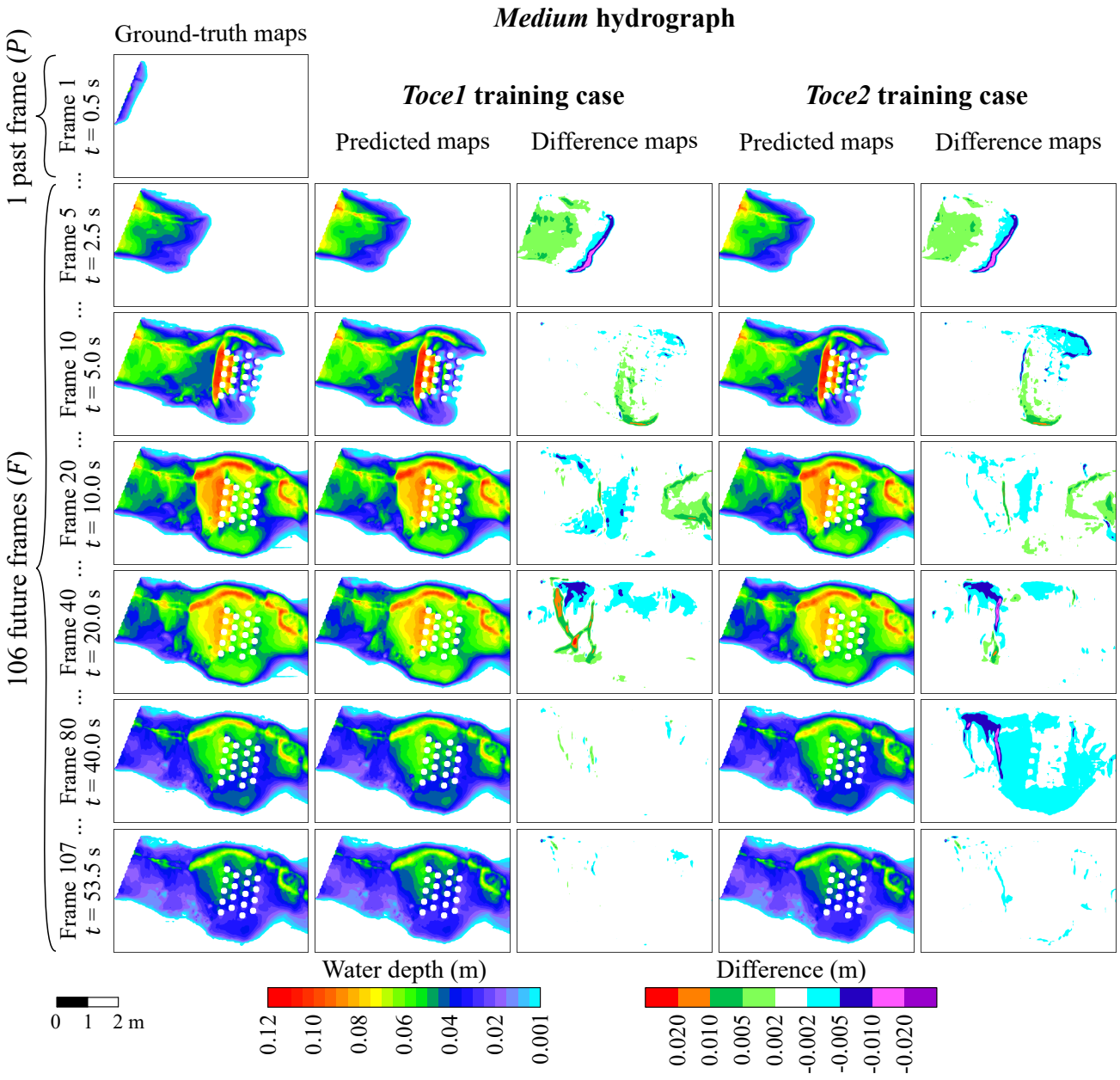

Figure S6. Toce River case study: comparison of predicted maps for the *Medium* hydrograph of the testing dataset using the surrogate model trained with the *Toce1* and *Toce2* configurations. The first column presents the ground-truth maps obtained from the hydrodynamic model. The second and fourth columns show the predicted maps for the *Toce1* and *Toce2* configurations, respectively. The third and fifth columns illustrate the differences between the predicted and target maps for the *Toce1* and *Toce2* configurations, respectively. Only selected representative instants are shown.

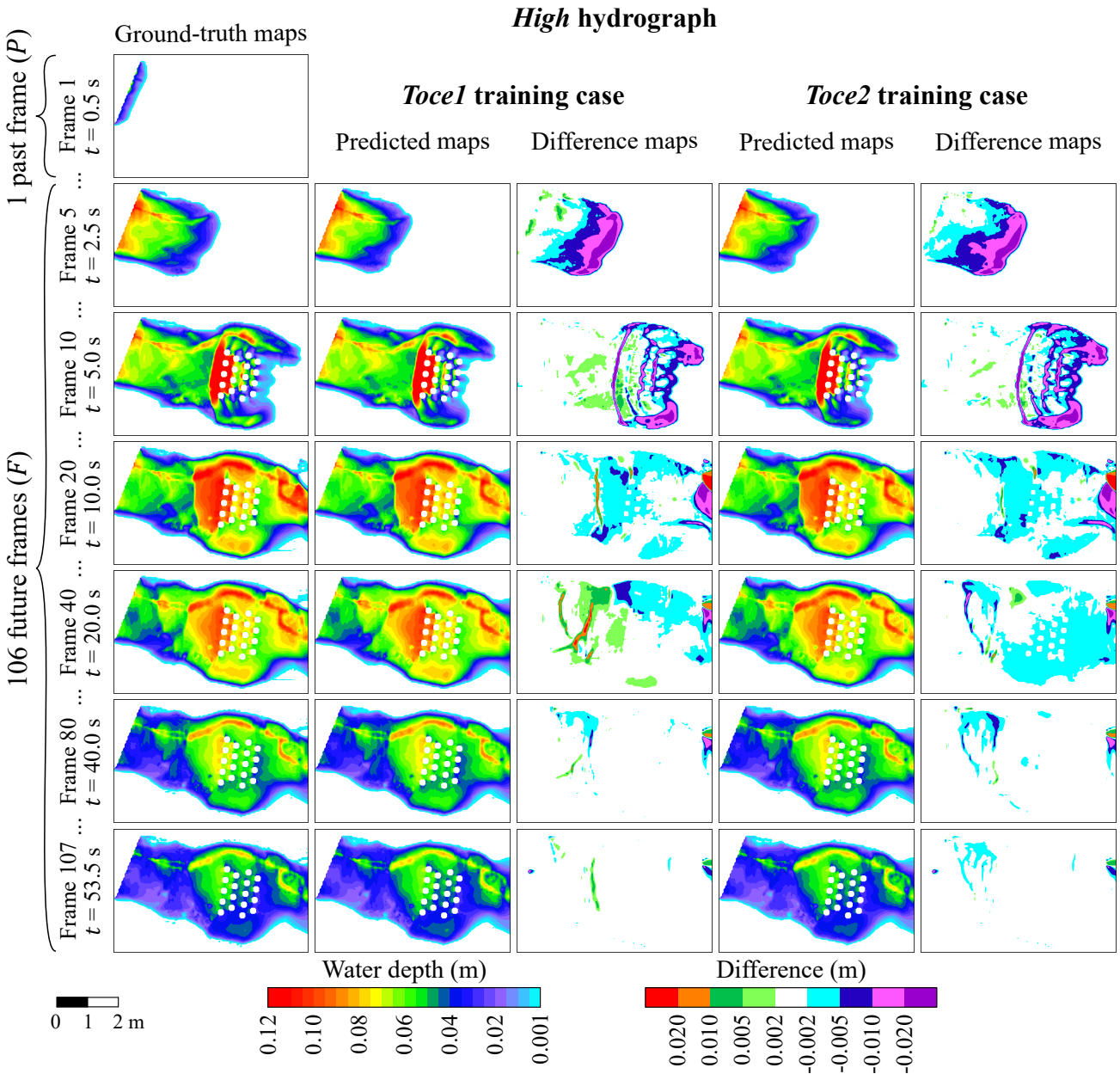

Figure S7. Toce River case study: comparison of predicted maps for the *High* hydrograph of the testing dataset using the surrogate model trained with the *Toce1* and *Toce2* configurations. The first column presents the ground-truth maps obtained from the hydrodynamic model. The second and fourth columns show the predicted maps for the *Toce1* and *Toce2* configurations, respectively. The third and fifth columns illustrate the differences between the predicted and target maps for the *Toce1* and *Toce2* configurations, respectively. Only selected representative instants are shown.

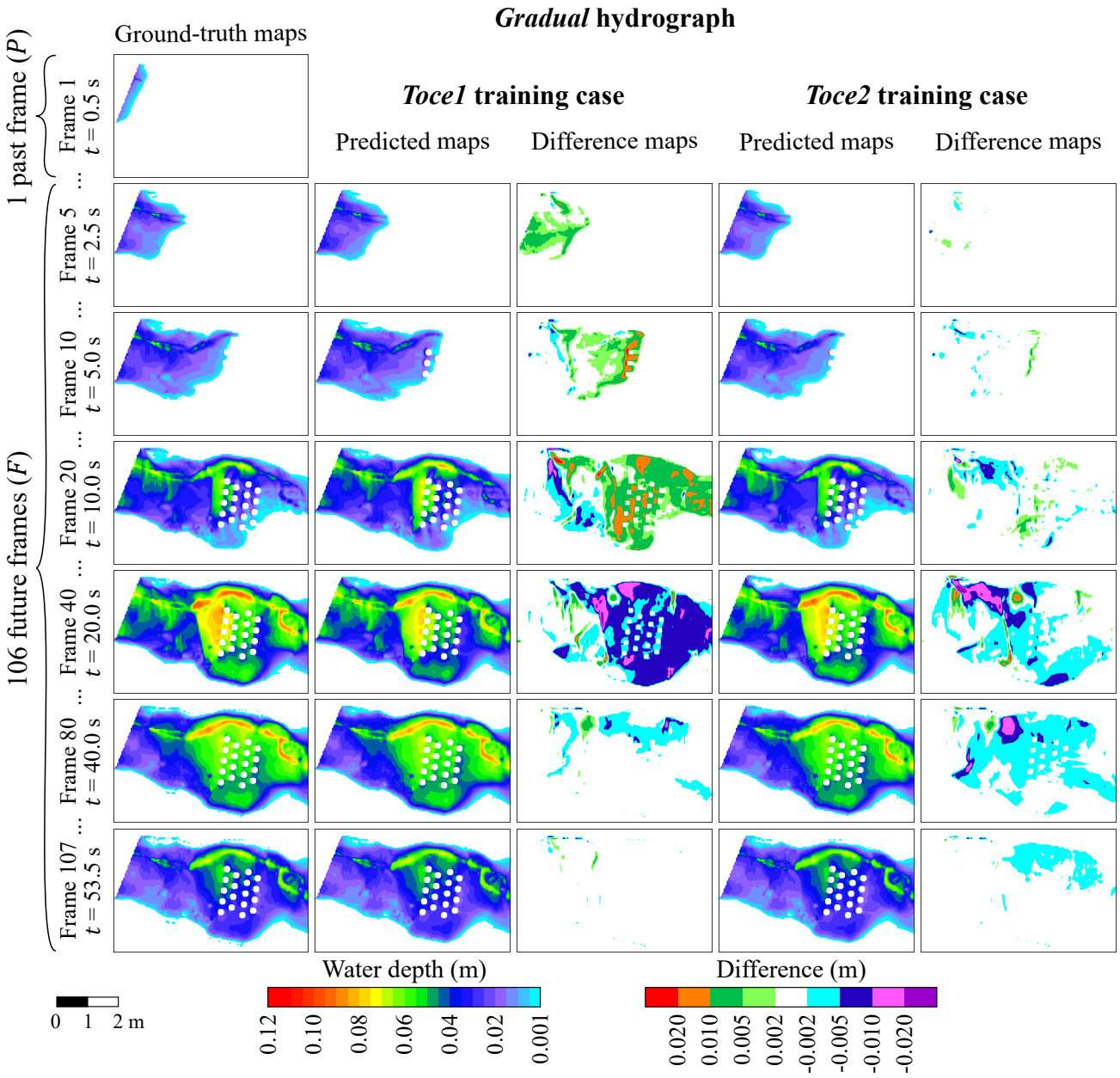

Figure S8. Toce River case study: comparison of predicted maps for the *Gradual* hydrograph of the testing dataset using the surrogate model trained with the *Toce1* and *Toce2* configurations. The first column presents the ground-truth maps obtained from the hydrodynamic model. The second and fourth columns show the predicted maps for the *Toce1* and *Toce2* configurations, respectively. The third and fifth columns illustrate the differences between the predicted and target maps for the *Toce1* and *Toce2* configurations, respectively. Only selected representative instants are shown.

S3: Po River case study: inundation maps for the *Po3* training configuration

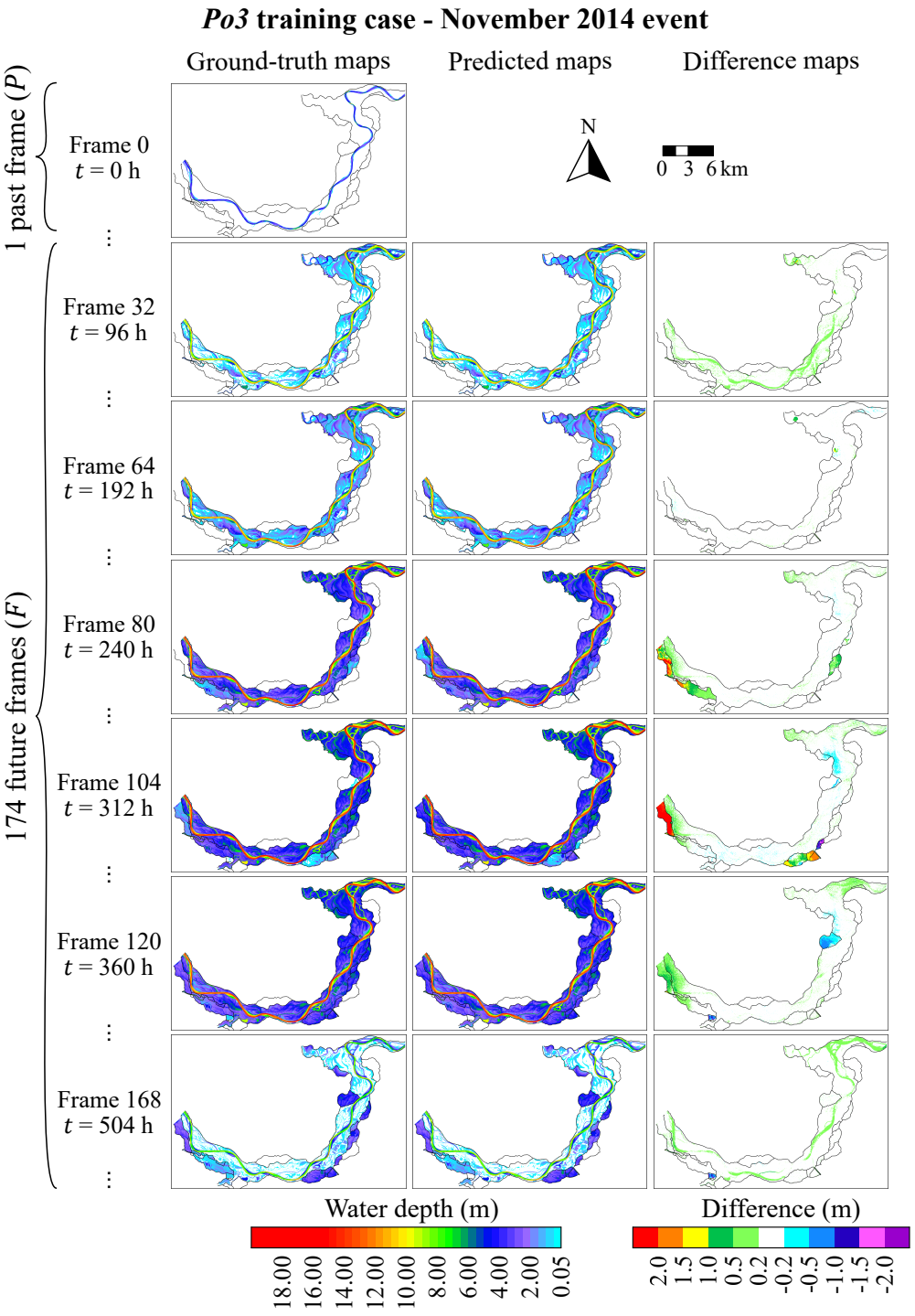

Figure S9. (Caption next page.)

Figure S9. (Previous page.) Po River case study: real-time forecasting of the November 2014 flood event using the FloodSformer model with the *Po3* training configuration. The columns represent, respectively, the ground-truth maps obtained from the hydrodynamic model, the maps predicted by the surrogate model, and the difference maps between the predicted and ground-truth maps. Only selected representative instants are shown.

References

Testa, G., Zuccalà, D., Alcrudo, F., Mulet, J., and Soares-Frazão, S.: Flash flood flow experiment in a simplified urban district, Journal of Hydraulic Research, 45, 37–44, https://doi.org/10.1080/00221686.2007.9521831, 2007.